NASA-CR-203765

Wind variability of B supergiants: II. The two-component stellar wind of γ Arae

IN ...

R.K. Prinja[1], D. Massa[2], A.W. Fullerton[3], I.D. Howarth[1] and M. Pontefract[1]

[1] Department of Physics & Astronomy, University College London, Gower Street, London WC1E 6BT, U.K.
[2] Applied Research Corporation, 8201 Corporate Drive, Landover, MD 20786, U.S.A.
[3] Max-Planck-Institut für Astrophysik, Karl-Schwarzschild-Str. 1, Postfach 15 23, 85740 Garching bei München, Germany

Abstract. The stellar wind of the rapidly rotating early-B supergiant, γ Ara, is studied using time series, high-resolution IUE spectroscopy secured over ~ 6 days in 1993 March. Results are presented based on an analysis of several line species, including N V, C IV, Si IV, Si III, C II, and Al III. The wind of this star is grossly structured, with evidence for latitude-dependent mass loss which reflects the role of rapid rotation. Independent, co-existing time variable features are identified at low-velocity (redward of ~ -750 km s^{-1}) and at higher-speeds extending to ~ -1500 km s^{-1}. The interface between these structures is 'defined' by the appearance of a discrete absorption component which is extremely sharp (in velocity space). The central velocity of this 'Super DAC' changes only gradually, over several days, between ~ -400 and -750 km s^{-1} in most of the ions. However, its location is shifted redward by almost 400 km s^{-1} in Al III and C II, indicating that the physical structure giving rise to this feature has a substantial velocity and ionization jump. Constraints on the relative ionization properties of the wind structures are discussed, together with results based on SEI line-profile-fitting methods. The overall wind activity in γ Ara exhibits a clear ion dependence, such that low-speed features are promoted in low-ionization species, including Al III, C II, and Si III. We also highlight that – in contrast to most OB stars – there are substantial differences in the epoch-to-epoch time-averaged wind profiles of γ Ara.

We interpret the results in terms of a two-component wind model for γ Ara, with an equatorially compressed low ionization region, and a high speed, higher-ionization polar outflow. This picture is discussed in the context of the predicted bi-stability mechanism for line-driven winds in rapidly rotating early-B type stars, and the formation of compressed wind regions in rapidly rotating hot stars. The apparent absence of a substantial shift in the wind ionization mixture of γ Ara, and the normal nature of its photospheric spectrum, suggests wind-compression as the likely dominant cause for the observed equatorial density enhancements.

1. Introduction

The coupling of mass loss and rotation potentially affects the structure and evolution of massive, hot stars. The winds, which may be distorted by rapid rotation, can play a role in removing angular momentum from stars, whilst rapid rotation alters the internal stellar structure, and may change observable characteristics such as the modes of nonradial pulsation. The effect of stellar rotation on radiatively-driven stellar winds is an important topic therefore, and one which has been boosted in recent years by several interesting developments, including, (i) detailed theoretical models describing the two-dimensional structure of winds from rotating hot stars (e.g. the 'Wind-Compressed Disk', WCD, models of Bjorkman & Cassinelli 1992, 1993, and the related hydrodynamical simulations of Owocki et al. 1993), (ii) the predicted bi-stability of radiation-pressure-driven winds (Pauldrach & Puls 1990) and the consequent possible formation of disks around rapidly rotating early-B stars (Lamers & Pauldrach 1991), (iii) observational evidence for cylindrically symmetric stellar winds in OB stars (e.g. Massa 1992, Howarth & Reid 1993, Bjorkman et al. 1994, Massa 1995, Reid & Howarth 1996), and (iv) results from the extensive IUE 'Mega Campaign' which indicate that stellar wind activity and structure in OB stars may be modulated by rotation (Massa et al. 1995a, Prinja et al. 1995, and Howarth et al. 1995).

In this paper we present an analysis of the effects of rapid rotation on the structure of the stellar wind of the early B-type supergiant, γ Ara (HD 157246; B1 Ib, Table 1). Time-series, high-resolution IUE spectroscopy is discussed using data collected over ~ 6 days in 1993 March. This star is an important candidate for studies of mass loss and rotation since it is luminous, has a substantial and variable stellar wind, and has

a projected rotation velocity ($v_e \sin(i)$) which is more than 150 km s^{-1} higher that the mean value for early-type supergiants (Table 1). Wind studies of B supergiants also benefit from being able to sample a wider range of unsaturated ions. Massa et al. (1995b) previously demonstrated this advantage in their study of HD 64760 (B0.5 Ib, the first paper in this series).

Also of interest in γ Ara are the reports of optical line-profile variability presented by Baade (1983) and Baade & Ferlet (1984). The latter study identified two periods, of 4.1 and 20.9 hours, which may be attributed to nonradial pulsations. In addition, weak emission humps straddle the observed Hα absorption line of γ Ara (e.g. Baade 1983), which are likely signatures of an equatorial density enhancement view approximately edge on (Petrenz & Puls 1996). In the X-ray band, *Einstein Observatory* detections (IPC; 0.16-4.0 keV) of the star indicate a luminosity, L_x, ~ 2.7 × 10^{31} ergs s^{-1} (e.g., Cassinelli et al. 1981 and Grillo et al. 1992). In the ultraviolet, Snow & Morton (1976) and Snow (1977) have described *Copernicus* UV spectra of γ Ara and recorded an O VI λ1032 absorption line trough extending to −500 km s^{-1}. Prinja & Howarth (1986) documented variability in 7 high-resolution *IUE* (archive) spectra, spanning ~ 4 years.

We present here the first investigation of systematic short time-scale (hourly) variability in the stellar wind of γ Ara. Section 2 provides a brief description of the *IUE* data set, which is followed in Section 3 by a discussion of the time-averaged photospheric and wind line profile morphology, with comparisons to other (selected) OB stars. Extensive stellar-wind variability is documented in Section 4, where we establish the properties of phenomenologically different forms of (co-existing) wind structure, and derive constraints from SEI line-profile modelling. These results support a two-component wind model of γ Ara which is discussed in Section 5.

Table 1. Stellar parameters

Parameter	Value	Reference
Spectral type	B1 Ib	1
V	3.34	1
$v_e \sin(i)$	230 km s^{-1}	2
M_v	−5.8 mag	3
T_{eff}	20,260K	3
$R/R_\odot$	23	3
v_∞	>1500 km s^{-1}	4
$T(rotation)$	5.0 days	(upper limit)

1: Hiltner et al. (1969); 2: Slettebak et al. (1975); 3: Humphreys & McElroy (1984); 4: This paper.

2. The *IUE* observations

We obtained 55 high-dispersion *IUE* spectra (λλ 1150-1950; R ~ 10^4) of γ Ara over almost 6 days in 1993 March. The mean

sampling time for the data is ~ 2.5 hours, except for two gaps of ~ 6.5 hours which occur close to the start and end of the time series. All the spectra were taken using the large aperture, each with a 30 sec. exposure. The spectra were extracted from the photometrically corrected images using the IUEDR reduction package (Giddings et al. 1995) in the manner described by Howarth & Prinja (1989).

The rectified mean *IUE* spectrum of γ Ara is shown in Figure 1. The prominent wind-formed lines are due to N V λλ1239, 1243, Si IV λλ1394, 1403 and C IV λλ1548, 1551. Additional interesting probes are provided by the low-ionization lines of C III λ1175, Si III λ1206, C II λ1335, and Al III λλ1855, 1863 (Section 4). Other spectral features of note are the Si III λλ1300 photospheric triplets which sample the wind-photosphere interface at this spectral type (Massa et al. 1992; Massa et al. 1995b), and the swathe of line blanketing between ~ 1500 and 1700Å due mostly to Fe II-III.

3. The time-averaged profile morphology

3.1. The photospheric spectrum

The wind lines in luminous B stars are very sensitive to the physical parameters of the star (Walborn et al. 1995). Therefore, in order to understand the wind lines in γ Ara, the star must be placed into context. Consequently, we begin by comparing its photospheric lines to those of normal B supergiants. Not only does this enable us to delineate the peculiarities of its wind lines, it also allows us to determine whether the UV photospheric spectrum is consistent with the optical classification and whether rapid rotation affects the atmosphere (as is the case in HD 93521, Massa, 1995).

In making the comparisons, extreme care must be used in normalising the different spectra. This is because B supergiants lack a true, line-free continuum anywhere in the SWP camera range. As a result, the usual approach of simply picking a few regions of line-free continuum and then normalising the fluxes with a smooth curve drawn through these points is problematic at best. Instead, we adopt a more physical approach to the normalisation.

To begin, we "spin up" the spectra to be compared to that of γ Ara. We use a simple rotational broadening algorithm which ignores the particulars of the line formation process. Interstellar lines were not removed beforehand, so these affect the broadened spectra. However, interstellar lines are easily identified in the γ Ara spectrum, so their impact on the broadened spectra is easy to assess. Once the general shapes of the strong lines agree, we create a differential extinction curve between γ Ara and the comparison star. This curve is then fitted by the parameterization scheme developed by Fitzpatrick & Massa (1990 - FM hereafter) to produce a set of physically meaningful smooth functions which can be used to adjust the comparison star to agree with γ Ara. There is, however, the additional complication of the degradation of the *IUE* instrumental response between the epochs of the observations of the program and comparison stars. Fortunately, the functional form of the degradation differs
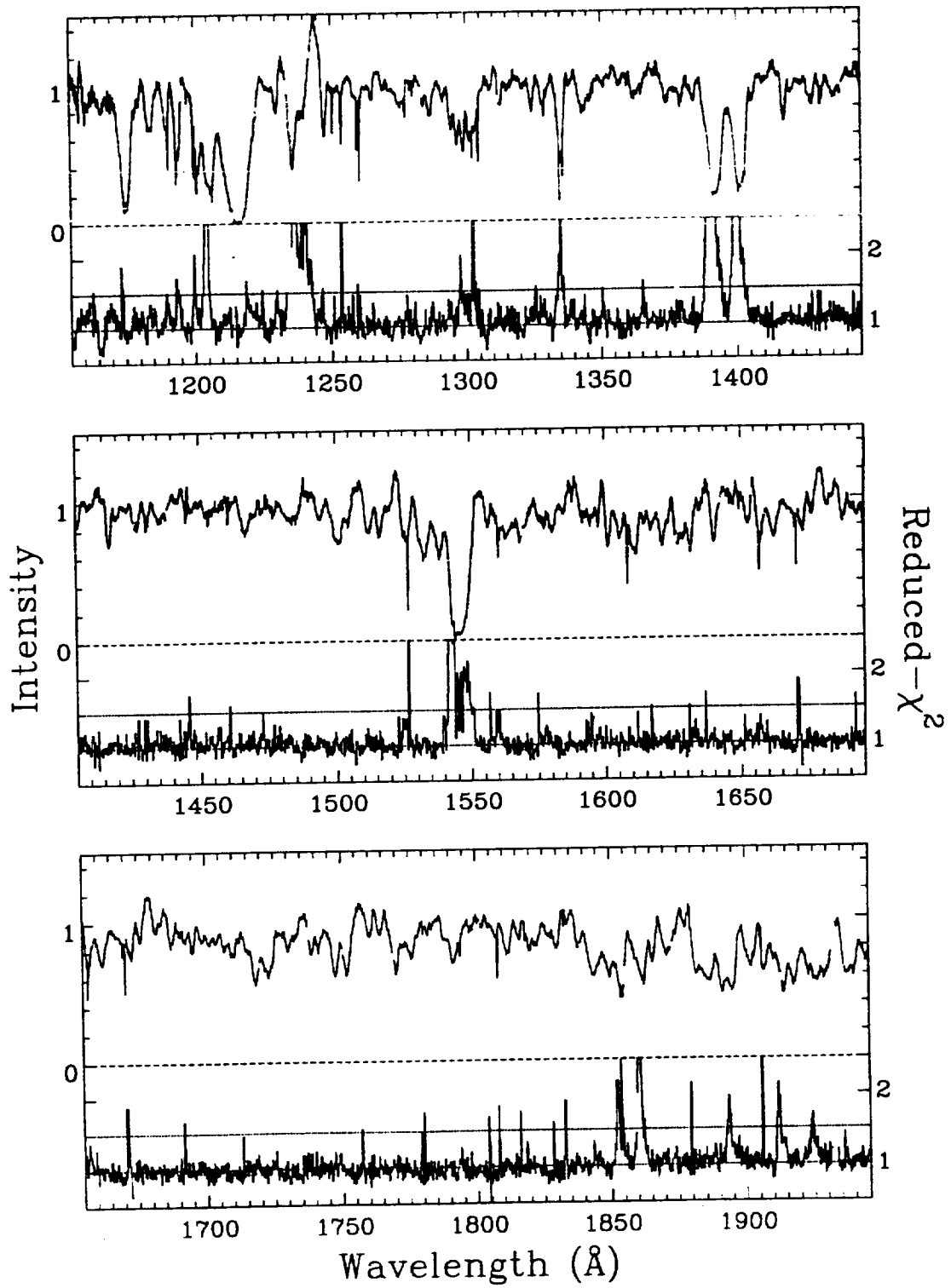
Fig. 1. The rectified mean-intensity and reduced-χ^2 spectra of γ Ara. The χ^2_ν spectrum has been lightly smoothed with a 3-point median filter; for points above the upper dotted line ($\chi^2_\nu \simeq 1.5$) the null hypothesis of constant normalised intensity may be rejected with 99% confidence (see Section 4).
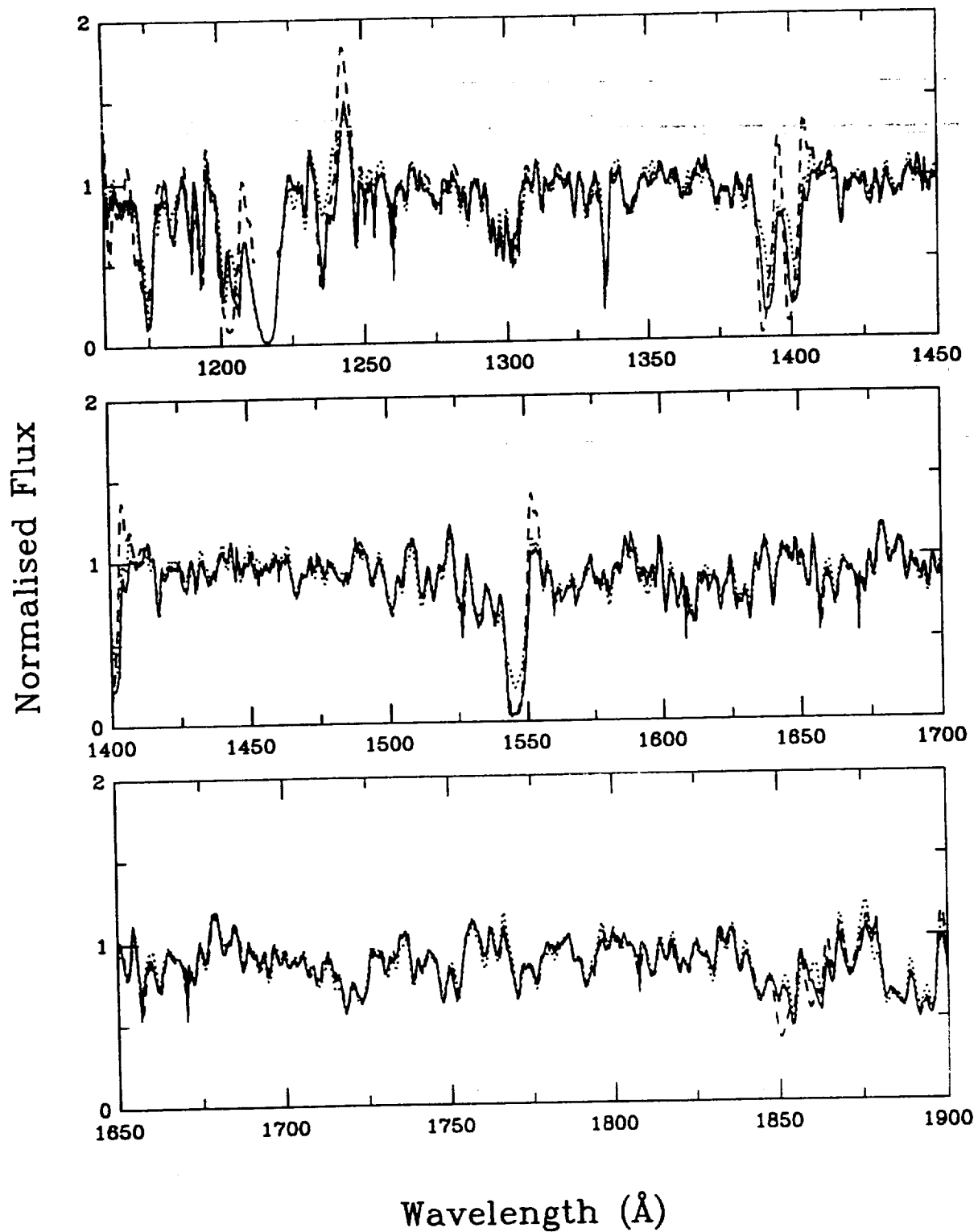
Fig. 2. Comparisons of normalised *IUE* SWP spectra of γ Ara (solid line), HD 109867 (B0.7 Ib; dashed line) and ζ Per (B1 Ib; dotted lines). (See also Appendix.)

considerably from the reddening functions, and it is possible to iterate to a consistent solution quickly. Finally, the spectra were corrected for differential Lyα absorption. The details of the corrections are described in the Appendix. Once these have been applied to the comparison stars, a *single* "continuum flux" can be estimated by drawing a smooth curve over the γ Ara spectrum and can then be applied to *all* the spectra. While there is reason to believe that this is not a true continuum, our approach ensures that it is consistent, and that all low-frequency differences in the flux distributions can be attributed to differences in the line blanketing. Note, however, that our treatment of the instrumental degradation is necessarily crude and that these corrections can be large shortward of ∼ 1265 Å(a procedure has not been officially adopted for this by the *IUE* Project). As a result, the relative shapes of the energy distributions shortward of 1265 Å should be given relatively less weight.

Figure 2 compares γ Ara, to rotationally broadened spectra of the normal B1 Ib star ζ Per and HD 109867 (B0.7 Ib). The classifications for the two comparison stars are from Walborn (1976). The observed $v \sin i$'s of ζ Per and HD 109867 are 50 and 90 km s^{-1}, respectively (Uesugi & Fukuda 1992). Both spectra were broadened by an additional 230 km s^{-1}. Since the effects of rotation add roughly quadratically, the equivalent $v \sin i$'s are 235 and 246 km s^{-1}. Additional broadening resulted in a clear mismatch of the profile shapes.

Either spectrum presents a good match to the photospheric lines in γ Ara, but the match with HD 109867 is spectacular – it is almost impossible to distinguish the dashed and solid lines in Fig. 2 over much of the spectrum. This is remarkable, considering that the spectra were broadened in a relatively simple manner.

Our comparison demonstrates that the UV *photospheric* spectrum of γ Ara is perfectly normal, and that it is intermediate between B0.7 and B1 Ib – probably a bit closer to the B0.7 Ib HD 109867. However, because MK types are bins, it may still be a legitimate B1 Ib, depending on exactly where the B0.7 Ib – B1 Ib boundary lies.

3.2. *The stellar-wind lines*

In this section we liken the observed time-averaged wind line morphology of γ Ara from our time series to those of selected hot stars to assess evidence for gross peculiarities, which may reflect the influence of rapid rotation. Figure 2 is also useful for assessing the peculiarities in γ Ara's wind lines. First, we note that *most* of its wind-line strengths are intermediate between those of ζ Per and HD 109867, but that its profiles are peculiar. For example, γ Ara's C IV λλ1550 absorption is as strong as it is in HD 109867, but the emission is closer to that in ζ Per. The same is true for Si III λ1206, Si IV λλ1400, and Al III λλ1860. The exception is N V λλ1240 emission, which is actually weaker in γ Ara, than *either* comparison star, although the absorption is about the same as in HD 109867.

The mean N V and C IV profiles of γ Ara are displayed in Figure 3, and compared to corresponding lines of HD 93521 (O9.5 V, $v_e \sin(i)$ ∼ 400 km s^{-1}) and ζ Oph (O9.5 V, $v_e \sin(i)$

∼ 351 km s^{-1}). The later two have been extensively studied for the effects of rapid rotation on the atmosphere and wind (see references in Section 1, and, e.g., Howarth et al. 1993, Massa 1995). The Si IV profile is essentially a function of luminosity class in hot stars (e.g., Walborn & Panek 1985), and so the comparison to γ Ara is only interesting for N V and C IV. Of special note is the step or 'shelf' identified in the blueward wing of the C IV profile in HD 93521 at ∼ −1000 km s^{-1}, which has been interpreted and modelled as due to the presence of an equatorial disk (Massa 1992, Howarth & Reid 1993 and Bjorkman et al. 1994). This type of structure is not so clear in the (mean or individual) C IV profiles of γ Ara. Interestingly, however, the two-component wind models of Bjorkman et al. (1994) predict that this profile step would only be present in the case of stars viewed very nearly edge-on, and for a thin equatorial 'disk'. The line profiles in Figure 3 also provide little or no evidence for *blueshifted* emission components in γ Ara (cf. Howarth & Reid 1993). Although this conclusion relies in part on the rather difficult continuum placements, it is supported, however, by the overall match obtained with the standard stars in Fig. 2. The N V emission strength in γ Ara exceeds that of ζ Oph and is almost comparable to that of HD 93521, whilst the C IV emission is not so exceptional. Finally, note that the mean profiles of γ Ara based on the 1995 archival data set discussed in Section 4.4, which excludes high-velocity material, provides a better overall 'match' to HD 93521 in Fig. 3.

We will see in the following section that it is the time-dependent behaviour of the wind lines, and the incidence of evolving wind structure, which provides the most powerful probe of latitude-dependent mass-loss in γ Ara.

4. Stellar wind variability and structure

Snow (1977) and Prinja & Howarth (1986) have previously noted that the UV resonance lines of γ Ara show changes in spectra separated by months to years. Most OB stars, when monitored with *IUE* over several days, show evidence for stellar-wind variability; it is not surprising, then, that the same is true for γ Ara. What is remarkable, however, is the complex nature of the line-profile changes found in our intensive time-series data, and what they reveal about the wind structure and geometry.

To carry out a rigorous search for statistically significant line-profile variability we have calculated the reduced-χ^2 spectrum of the normalised data:

$$\chi^2_\nu(\lambda) = \sum \left\{ \frac{f_i(\lambda) - \overline{f}(\lambda)}{\sigma(f, \lambda)} \right\}^2 \Big/ (N - 1) \qquad (1)$$

where the standard deviation of the N spectra, $\sigma(f, \lambda)$ is calculated in the manner described by Howarth & Smith (1994). The results are included in Fig. 1.

The narrow 'spikes' in the reduced-χ^2 spectrum are attributable to undersampling of narrow interstellar lines, or to instrumental effects. However, a range of stellar features show clear evidence for statistically significant variability
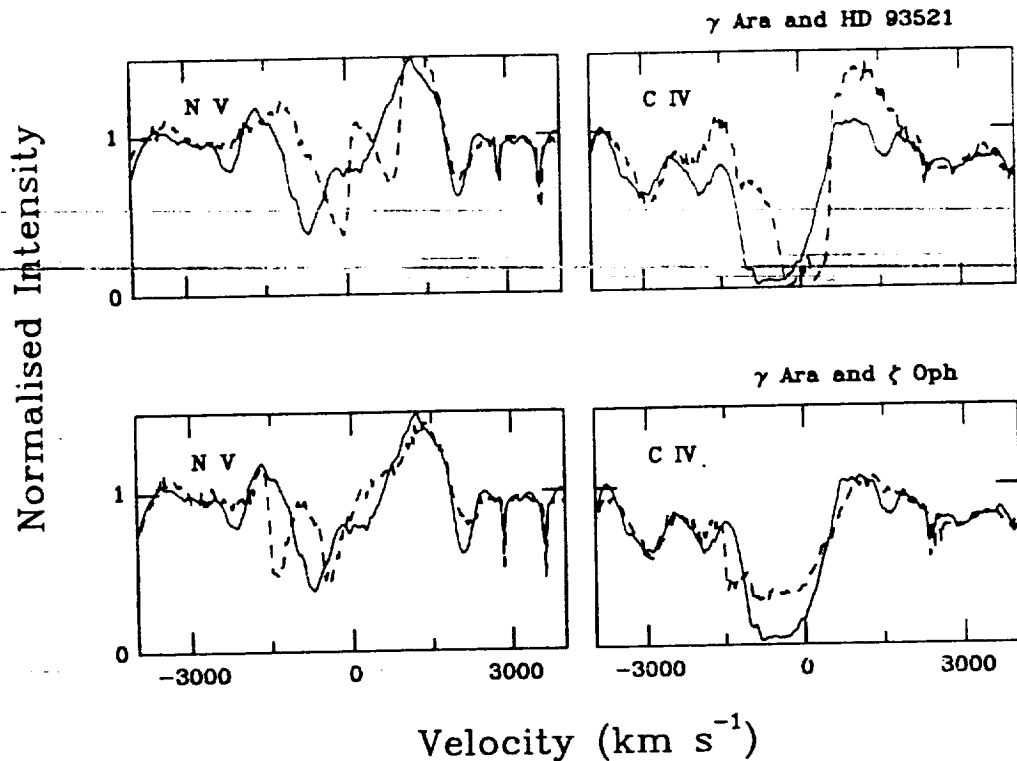
Fig. 3. The mean N V and C IV wind lines of γ Ara from our time series (solid lines) are compared to the corresponding profiles (dashed lines) of HD 93521 (O9.5 V, $v_e \sin(i) \sim 400$ km s^{-1}) and ζ Oph (O9.5 V, $v_e \sin(i) \sim 400$ km s^{-1}).

(with $\geq 99\%$ confidence). Those features are: Si III $\lambda1206.5$Å; N V $\lambda\lambda1238.8$, 1242.8Å; Si III multiplet UV4 ($\lambda\lambda1294.6$-1303.3Å); C II $\lambda\lambda1334.5$, 1335.7Å; Si IV $\lambda\lambda1393.8$, 1402.8Å; C IV $\lambda\lambda1548.2$, 1550.8Å; Al III $\lambda\lambda1854.7$, 1862.8Å; and Fe III multiplet UV34 ($\lambda\lambda1895.5$-1926.3Å).

Most of these lines correspond to ground-state transitions, but it is particularly interesting that the 'photospheric' Si III UV4 multiplet shows significant variability which demonstrates that the lines are formed, at least in part, in the stellar wind. The only 'wind' feature not found to show significant variability is C III $\lambda1175$, but the signal level at such short wavelengths is low in IUE data, and hence the sensitivity to variability is also low. The large number of stellar-wind lines, and the range of ionization potential spanned by their parent ions, affirm our earlier assertion of the suitability of B supergiants for stellar-wind studies.

Two-dimensional grey-scale representations of the line profile changes in Si IV, C IV and N V, plus Si III, C II and Al III are shown in Fig. 4. In each case the data were normalised by a minimum absorption (maximum flux) template, such that darker shades in Figure 4 represent greater line optical depth. The IUE data set of γ Ara provides an excellent example of how these 'imaging' techniques can reveal details of evolving wind structure which are almost impossible to discern from a simple inspection of the observed line spectra. Some salient points are immediately apparent from this figure:

1. The wind of γ Ara is extensively structured and highly time variable. Some, but not all, of the characteristic features are present in several ion species.

2. A remarkable signature in all the spectral lines in Fig. 4 is the presence of a discrete absorption component (DAC) which is extremely narrow (in velocity space; see section 4.1). It is detected in the higher-ionization species at the start of the observing run at ~ -400 km s^{-1}, and gradually evolves bluewards to a maximum displacement at ~ -750 km s^{-1} over more than 3.5 days. The feature becomes difficult to track after this time period since it then blends with other variable structures. This 'Super DAC' is considerably sharper than DACs seen in the middle, or shortward edges, of absorption troughs in OB stars. Only one such feature is apparent in Figure 4; it does not recur during the $\sim$ 6 days of observations, though it may persist (with variable strength) for more than 4 days (section 4.1).

3. The central velocity of the 'Super DAC' is, however, clearly displaced several hundred km s^{-1} further to the blue in Si IV, C IV and N V than in Al III and C II (Section 4.1).

4. Weaker, less discrete, variability is also present at high velocities (up to ~ -1500 km s^{-1}) in the high-ionization species. Variations in the low-ion species in γ Ara are mostly confined to the velocity 'boundary' defined by the 'Super DAC' however.

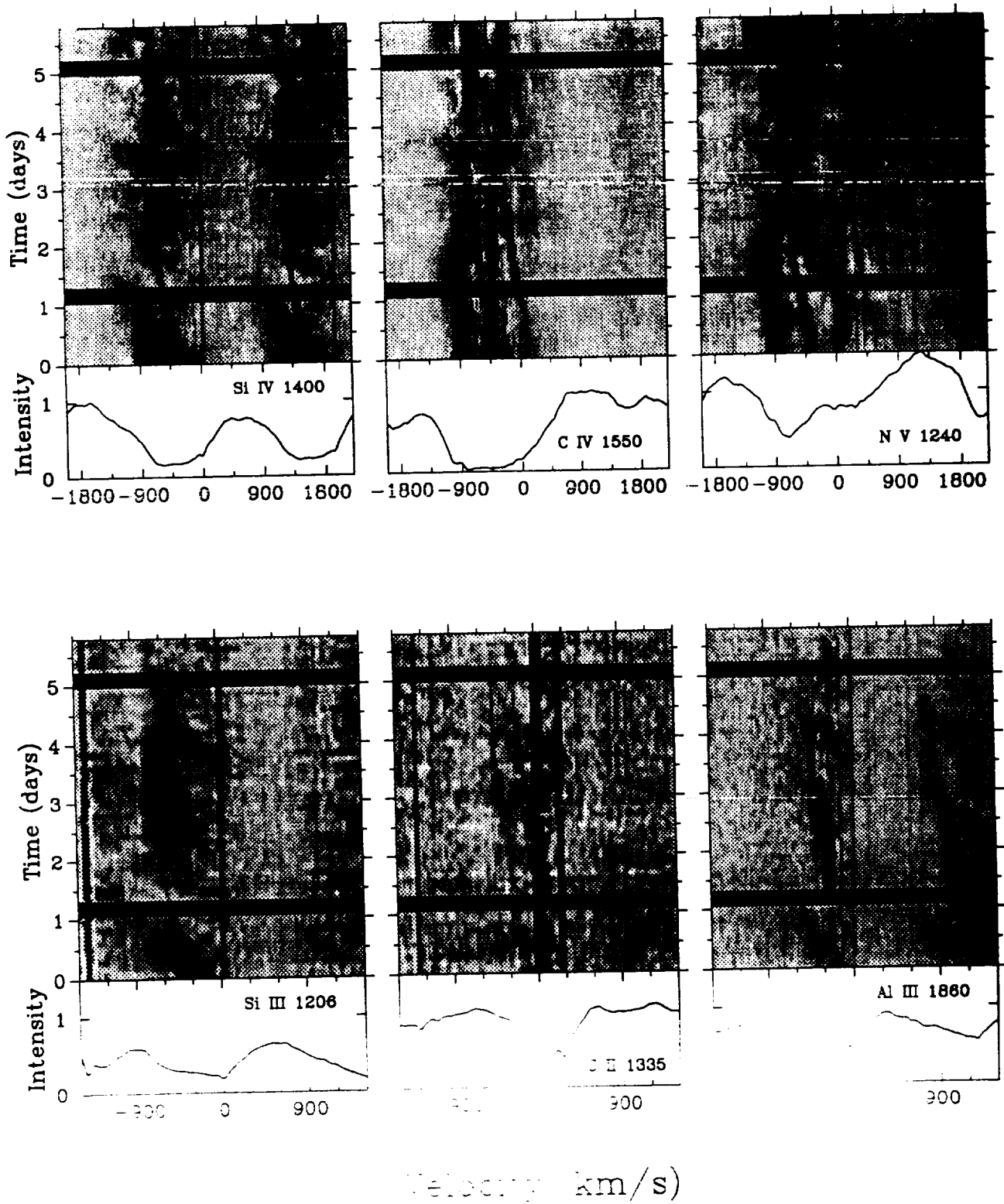5. In most cases of OB star winds, the discrete absorption components (which diagnose the structure) migrate bluewards

Fig. 4. Grey-scale representations of line profile variations in ~ Ara. Individual time-series spectra have been normalised by a minimum absorption (maximum flux) template. The spectra are therefore darkest where the line optical depths are greatest. Mean line profiles are shown in the panels below each grey-scale. In the case of doublets, the velocity scale is with respect to the blue component.
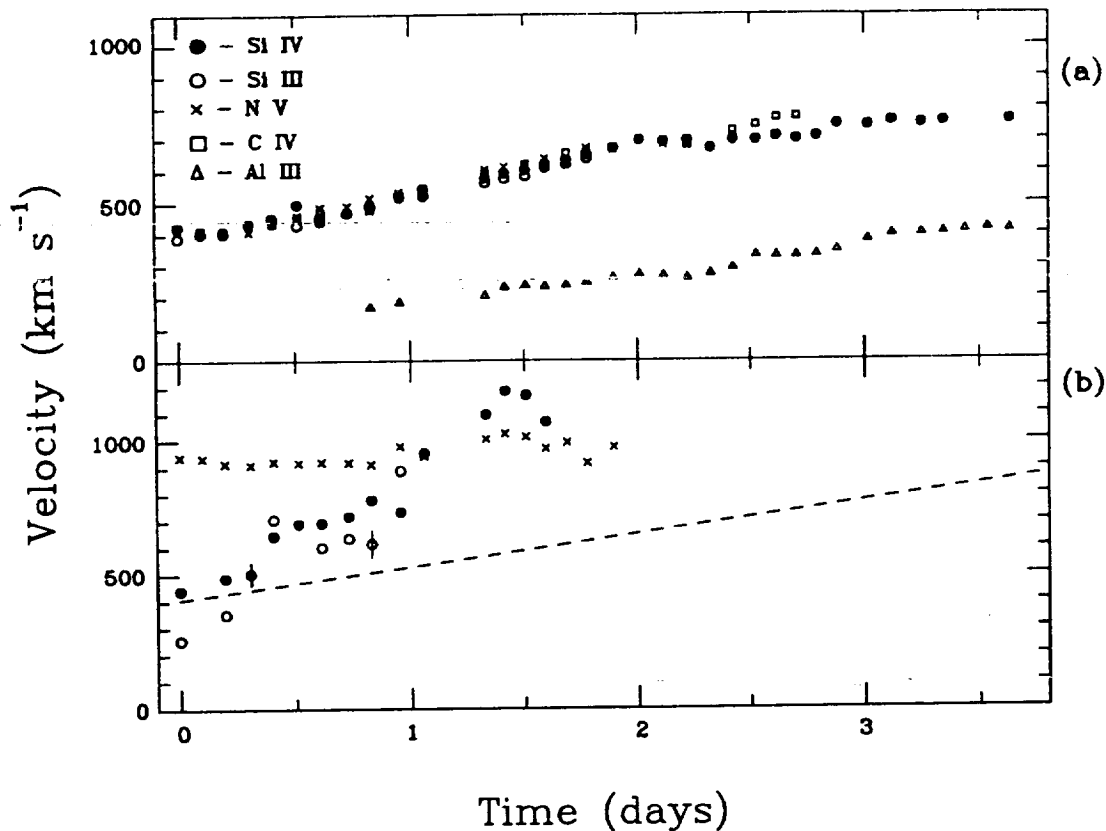
Fig. 5. (a) The central velocity of the 'Super DAC' is shown as a function of time for Si IV (filled circles), Si III (open circles), N V (crosses), C IV (open squares), and Al III (open triangles). (b) The velocity behaviour of high-speed structures evident between T = 0 and 1.5 days (cf. Fig. 4). The different symbols have the same meaning as in (a). The mean velocity of the 'Super DAC' in Si IV, Si III, N V and C IV is also shown (dashed line).

to an asymptotic velocity which can be identified with the wind terminal velocity (e.g. Prinja et al. 1990). Usually, the only profile variations evident beyond the DAC terminal velocity are due to fluctuations in the shortward profile edge of saturated resonance lines. These changes may be associated with, microturbulent, motions or shocks (e.g. Lucy 1982, 1983 and Owocki et al. 1988). The observation in γ Ara of localised ion-dependent variability extending beyond the maximum velocity of the 'Super DAC' is unique; it indicates spatially independent structures, and likely points to a two-component stellar wind. This notion is developed further in the remainder of this paper.

4.1. DAC velocities

In order to derive quantitative measures of enhancements seen in the wind lines, the DACs were modelled using least squares Gaussian profile fits, with the central velocity (v_c), full-width at half-maximum (FWHM), and central optical depth (τ_0) as the free parameters (see e.g. Howarth & Prinja 1989). We concentrated on matching (in different ions) the well defined 'Super DAC', and the best resolved of the high-velocity structures, which is present for about 1.5 days from the start of the obser-

vations, between ~ −500 km s^{-1} and −1500 km s^{-1}. The combination of larger optical depth in the C IV absorption trough, and additional noise, results in inconsistent fits to wind features in this line. We therefore only quote here 'by eye' estimates of DAC velocities in C IV.

The observed central velocities of the 'Super DAC' are plotted in Fig. 5(a) for five spectral lines; only very rarely in studies of hot star winds is it possible to monitor variable structure in such a wide range of ions. The velocity evolution of this exceptionally localised feature is essentially identical in Si III, Si IV, N V and C IV, from ~ −400 to −750 km s^{-1} over ~3.5 days. We cannot reliably measure the feature beyond this time, though the images in Fig. 4 suggest that the 'Super DAC' persists for more than 4 days. Applying a linear model to the velocity versus time data in Fig. 5(a) for these ions gives a mean acceleration of ~ 1.57 × 10^{-3} km s^{-2} (s.d. = 0.22 × 10^{-3} km s^{-2}). This acceleration is lower than is typical for DACs seen at intermediate velocities in OB stars (e.g. Prinja 1994), where they are already no more than 50% of the values predicted by steady-state wind models. The general agreement between the velocities of these four ions in Fig. 5(a) is in stark contrast with the structure in Al III λ1855. The 'Super DAC' in Al III is displaced systematically redward by ~ 400 km s^{-1}

relative to the other ions (see also Fig. 4). To the best of our knowledge this is the first clear case of a discrete enhancement in an OB star wind whose velocities do not agree in different spectral lines. Remarkably, however, the velocity behaviour of the 'Super DAC' in Al III mirrors very well the trends observed in the other lines, and the overall acceleration of the feature in Al III ($\sim 1.07 \times 10^{-3}$ km s^{-2}) is broadly similar to that measured in the higher ions. The full-width at half-maximum of the 'Super DAC' is typically only $\sim$ 80 – 230 km s^{-1}, with no obvious trend as a function of ion species. Note also that 'Super DAC' in C II λ1334.5 appears at the same velocities as in Al III (Fig. 4). It seems therefore that the same physical structure is responsible for the formation of the 'Super DAC' in all the lines (including Al III and C II), but it has a velocity jump of at least 400 km s^{-1}. This behaviour may relate to the action a substantial spatially confined shock region in the wind, where the post-shock gas is denser, lower speed, and less highly ionized than the pre-shock material. Mullan (1984) and Cranmer & Owocki (1996) discuss some pertinent models which may potentially result in velocity jumps of several 100 km s^{-1}.

As shown earlier, another remarkable aspect of the variability in γ Ara is that variable wind structure is present beyond the 'terminal velocity' of the 'Super DAC'. These high speed features are considerably broader (FWHM $\sim$ 450 – 900 km s^{-1}) and more tenuous in appearance (Fig. 4). The central velocities of the most clearly recorded feature in our data set (between T = 0 and 1.5 days) are shown in Fig. 5(b) for Si IV, Si III and N V. We are unable to record it confidently in C IV (mostly due to doublet merger and the deep absorption trough) and in Al III (where it may be only very weakly present at the lowest velocities, if at all). This structure exhibits a blueward progression between $\sim$ −300 and −1200 km s^{-1} in Si IV and Si III only, where it has a higher acceleration ($\sim 5.88 \times 10^{-3}$ km s^{-2}) than the 'Super DAC'. A better defined, stronger, feature is present during this time period in N V at $\sim$ −950 km s^{-1}, but it exhibits little evidence for systematic central velocity changes. Traces of similar high-velocity structures are evident at other times during the observing run, and we estimate that the maximum observed velocity reached by the high speed material is $\sim$ −1500 km s^{-1} (see e.g. T $\sim$ 4 days in Si IV; Fig. 4).

Overall, these results project a picture of substantial coherent wind structures in γ Ara, which co-exist but which develop on separate time scales.

4.2. Relative ion behaviour

It is already apparent from e.g. Fig. 4 that the low ion species, plus Si III and Si IV, exhibit low-velocity structures in γ Ara which are mostly bounded in velocity space by the 'Super DAC'. Discrete, higher-velocity variations (i.e., blueward of −750 km s^{-1}) are also noted however in C IV, N V, and Si IV. We examine here the relative ion behaviour of material responsible for the fluctuations in both these velocity domains.

Following the methods of our previous UV studies of structure in OB stars, we estimated the column density of material
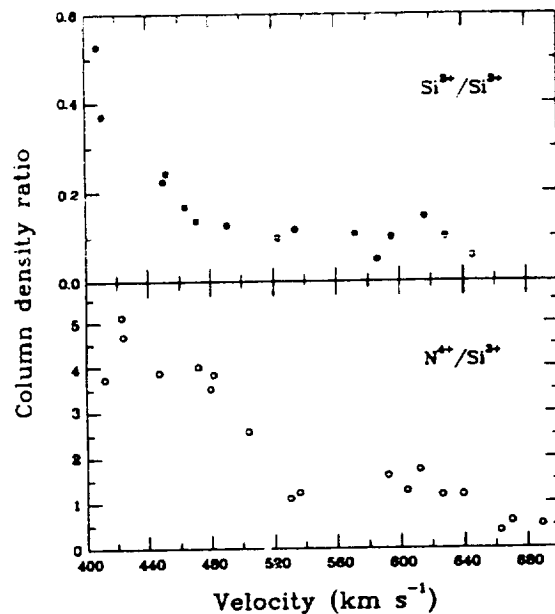

Fig. 6. The observed variation in the 'Super DAC' ion density ratios of Si^{2+}/Si^{3+} and N^{4+}/Si^{3+} as a function of central velocity.

responsible for the DACs, which may be expressed in terms of the Gaussian fitting parameters and atomic constants, and determined using plane-parallel geometry (e.g. Howarth & Prinja 1989). The mean ion column densities (dex cm^{-2}; over all velocities) of the 'Super DAC' are: Si^{2+}, 12.91; Si^{3+}, 13.87; N^{4+}, 14.00; and Al^{2+}, 13.21. In all cases the densities vary by up to a factor of 2 during the time series. The relative ion fractions (and fitted central optical depth ratios) Si^{2+}/Si^{3+} and N^{4+}/Si^{3+} for the 'Super DAC' gradually decrease as a function of velocity between $\sim$ −400 and −700 km s^{-1} (Fig. 6). A comparison to Al^{2+} is not so useful since the feature is present at a substantially different velocity in this ion (Fig. 5a).

The column densities of the high-velocity structures (Section 4.1) are typically a factor of $\sim$ 3 larger in Si^{3+}, Si^{2+} and N^{4+} than in the (lower velocity) 'Super DAC'. The corresponding (cf. Fig. 6) mean ionization ratios for the high-speed material are Si^{2+}/Si^{3+} $\sim$ 0.13 ($\bar{v} \sim$ −710 km s^{-1}) and N^{4+}/Si^{3+} $\sim$ 3.6 ($\bar{v} \sim$ −1040 km s^{-1}). The higher ionization species are clearly favoured at high velocities.

To demonstrate this point further, we examined the observed fluxes in N V, C IV, Si IV, Si III and Al III at carefully chosen times and velocities to sample high- and low-velocity structures. Firstly, we measured the N V, C IV and Si IV fluxes ($F_{structure}$) in a velocity bin between −1200 and −800 km s^{-1}, during the time interval, T = 3.54 to 3.84 days (i.e., SWPs 47196 - 47205). This period corresponds to the incidence of a high-speed feature (Fig. 4). Secondly, to sample a low-speed event, we measured the N V, C IV, Si IV, Si III and Al III fluxes between −300 and −150 km s^{-1} during T = 3.73 to 3.95 days (i.e., SWPs 47202 - 47208). In both cases the observed fluxes were then normalised
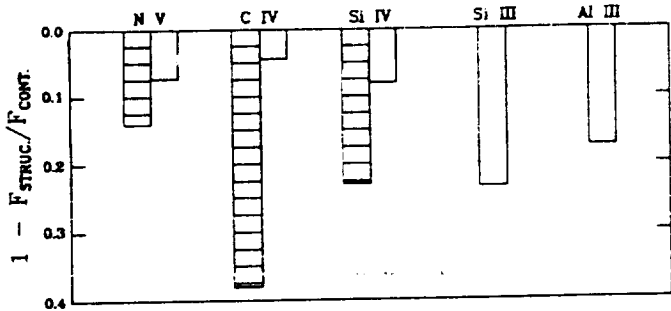
Fig. 7. The relative amount of absorption in high-velocity structures (between −1200 and −850 km s⁻¹; T = 3.53 - 3.84 days) is shown in the shaded histograms for several spectral lines. These are compared (in the open histograms) to values for low-velocity features (i.e. between −300 and −150 km s⁻¹; T = 3.73 - 3.95 days). All the fluxes (F_{struc}) have been normalised by the mean values measured, over the same velocity bins, during times when the wind is in a relatively quiet state (F_{cont}, Section 4.2).

by measurements made over the same velocity bins, but during times when little or no wind activity was evident (= $F_{continuum}$, i.e. T = 4.2 - 4.7 days and 3.2 - 3.5 days, for high- and low-speed bins, respectively).

The relative amount of absorption in the high- and low-velocity structures (= $1 - F_{structure}/F_{continuum}$) is shown for several lines in Fig. 7 as histograms (the shaded regions represent the high-velocity enhancements). For N V, C IV and Si IV the relative absorption due to the high-velocity material is greater than is the case for the low-velocity events. The enhancements due to high-speed structures in these ions are more pronounced therefore than the low-speed ones. The Si III and Al III line profiles do not extend beyond about −900 km s⁻¹, and cannot diagnose the high-velocity features. The absorption in the low-velocity bands, normalised to values when the wind is 'quiet', is greater in Si III and Al III compared to the higher ion species. The tentative implication here might be that the low-velocity structures are more prominent in the low-ionization species.

The overall picture of γ Ara presented by these IUE time series data is therefore of a two-component stellar wind, with a highly-ionized, high-speed region which favours N V, C IV, and Si IV, and a low-ionization, low-speed part showing more prominent structures in Si III, Al III and C II (with traces in Fe III).

4.3. Constraints from line-profile modelling

Some results from line-profile modelling are presented in this section in order to assess further the relative ionization properties of low- and high-speed wind material in γ Ara. We used the 'Sobolev with Exact Integration' method (SEI) described by Lamers et al. (1987), but with the modification previously employed in our study of HD 64760 (Massa et al. 1995b). Therefore, in addition to the usual velocity-law parameteri-

sation and provision for input photospheric spectra, the wind optical depth, $\tau_{rad}(w)$, was modelled in terms of ten independent, variable bins, the fit always progressing redward during the attempted profile match. The considerably greater freedom afford by this (arbitrary) model is preferred since our primary aim here is to sample the observed absorption optical depth due to structure in a stellar wind that is clearly not in steady-state. We acknowledge, however, that these methods are not entirely valid for time-dependent wind structures, particularly since a monotonic velocity law is assumed. The results in Fig. 5 may already point to a more complex relation between the velocity of wind features in γ Ara and their radial distance from the star.

Profile fits to the mean γ Ara line profiles from our time series are shown in Fig. 8(a), for Si III λ1206, N V λλ1240, Si IV λλ1400, and C IV λλ1550. (The Si III and N V profiles were corrected for 4.5 × 10²⁰ cm² Ly α absorption using a theoretical fully damped profile, in the manner of Bohlin et al. 1978). For each spectral line we approximated the input photospheric spectrum by adopting the 'spun up' IUE profiles of HD 37018 (B1 V) as a 'standard' (Fig. 8a). The corresponding optical depth bins, $\tau_{rad}(w)$, are shown in Fig. 8(b). For Si IV and C IV the optical depths are unconstrained redward of about 0.7 v_∞, but otherwise a 'match' may be claimed for Si III and N V down to about 0.4 v_∞ (see below). Its apparent from Fig. 8(a) that - despite the freedom of the model - there is a general excess of observed absorption at low velocities. An alternative view of course is that there is a lack of low-velocity wind emission in γ Ara, as may be the case for a non-spherical wind, where some of the 'expected' low-speed emission (above the poles) is weak or not present. Note that an excess of predicted scattered light at low velocities was also noted for the case of HD 64760 (Massa et al. 1995b), where highly asymmetric mass-loss is not suspected. A qualitative difference, however, is that we are unable to match the emission components in γ Ara for low ionization lines like Si III, which may be more confined in this case to the equatorial plane. An additional complication is that Puls et al. (1993) have shown that blue-shifted (forward scattered) emission will be removed by back-scattering at multiple resonance surfaces due to a nonmonotonic velocity field.

Examples of profile fits to individual Si III and N V profiles of γ Ara are shown in Fig. 9, spanning most of the time sequence of observations. These comparisons suggest that the lowest-velocity optical-depth bin which may be sampled is about 0.4 v_∞, and the bin at 0.7 v_∞ (for example) is a good indicator for high velocity material. Matches were attempted to all the individual Si III and N V profiles in our data set, and the observed optical-depth ratios of N⁴⁺/Si²⁺ are plotted as a function of time in Fig. 10, for high- and low-speed material (0.7 and 0.4 v_∞, respectively). It is clear once again (cf. Section 4.2) that the higher-ion species dominate in the fastest wind material, with the Si III optical depth excelling in the low-velocity regime. The overall mean ratios of N⁴⁺/Si²⁺ are ∼ 1.83 (s.d. = 0.84) and ∼ 0.25 (s.d. = 0.16) at 0.7 and 0.4 v_∞, respectively. There is also a tentative indication (Fig. 10) for an overall decrease in the N⁴⁺
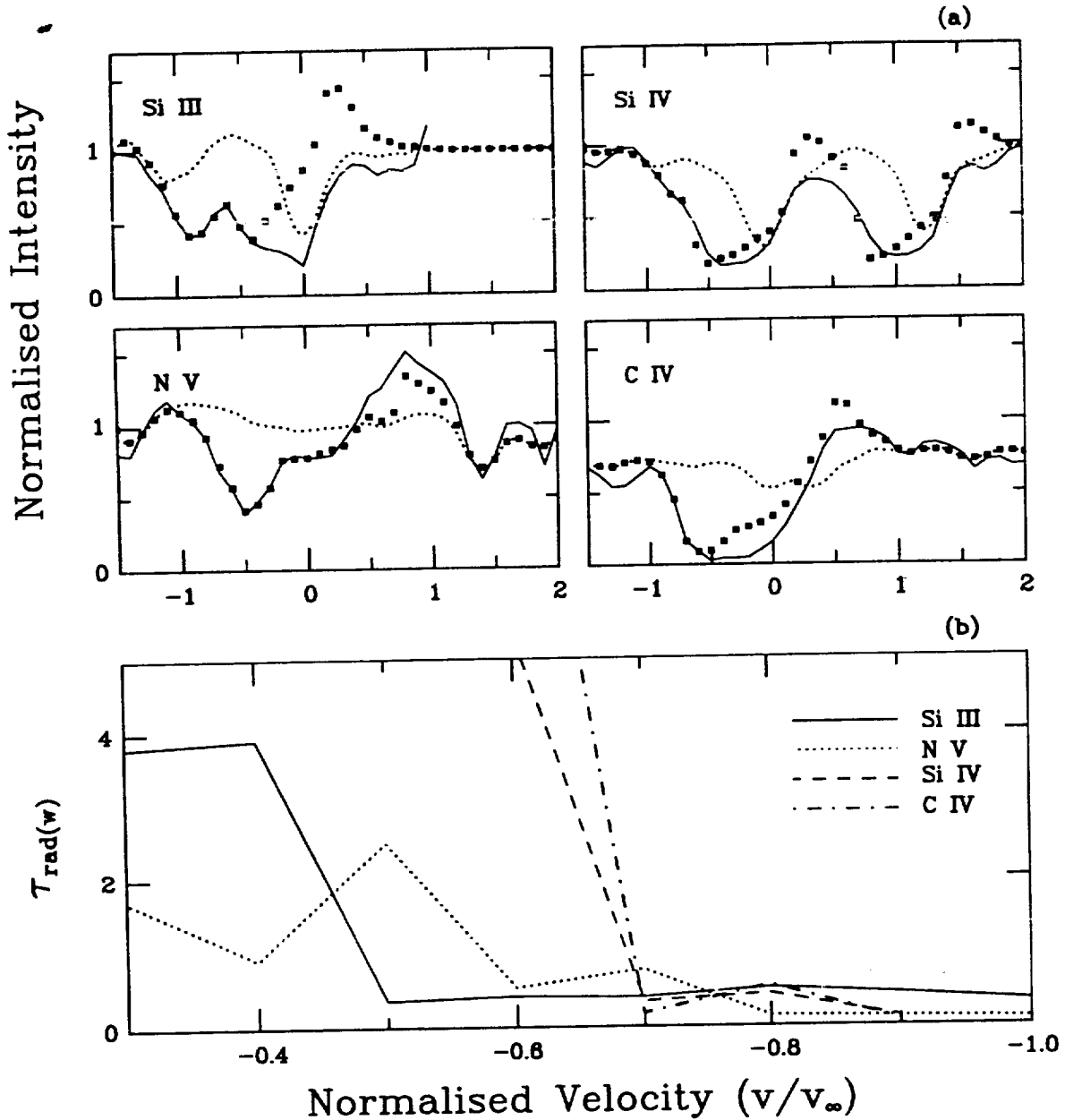
Fig. 8. (a) SEI model profile fits to the mean line profiles of γ Ara from our time series (filled squares and solid lines, respectively). We employed the SEI fitting method described by Massa et al. (1995b), with a wind terminal velocity $= 1500$ km s^{-1}. The dashed lines are the input photospheric spectra adopted by 'spinning up' the IUE profiles of HD 37018 (B1 V). (b) The corresponding wind optical depths, $\tau_{rad}(w)$, for Si III (solid line), N v (dotted line), Si IV (dashed line), and C IV (dot-dashed line).

optical depth at high velocities during the progression of the ~ 6-day time series.

This two-component nature of the wind in γ Ara is discussed further in Section 5, together with the potential roles of the mechanism for bi-stable radiation driven winds and the formation of compressed wind regions.

4.4. Long term variations

In this section we consider how the wind of γ Ara during our 1993 observing run compared to other (archive) observations. Prior to the 1993 series, 7 spectra were obtained between 1978 and 1982 (see e.g. Prinja & Howarth 1986). In 1995 March, a sparsely sampled 17 day time series was obtained in order to determine the persistence of wind structures and to assess
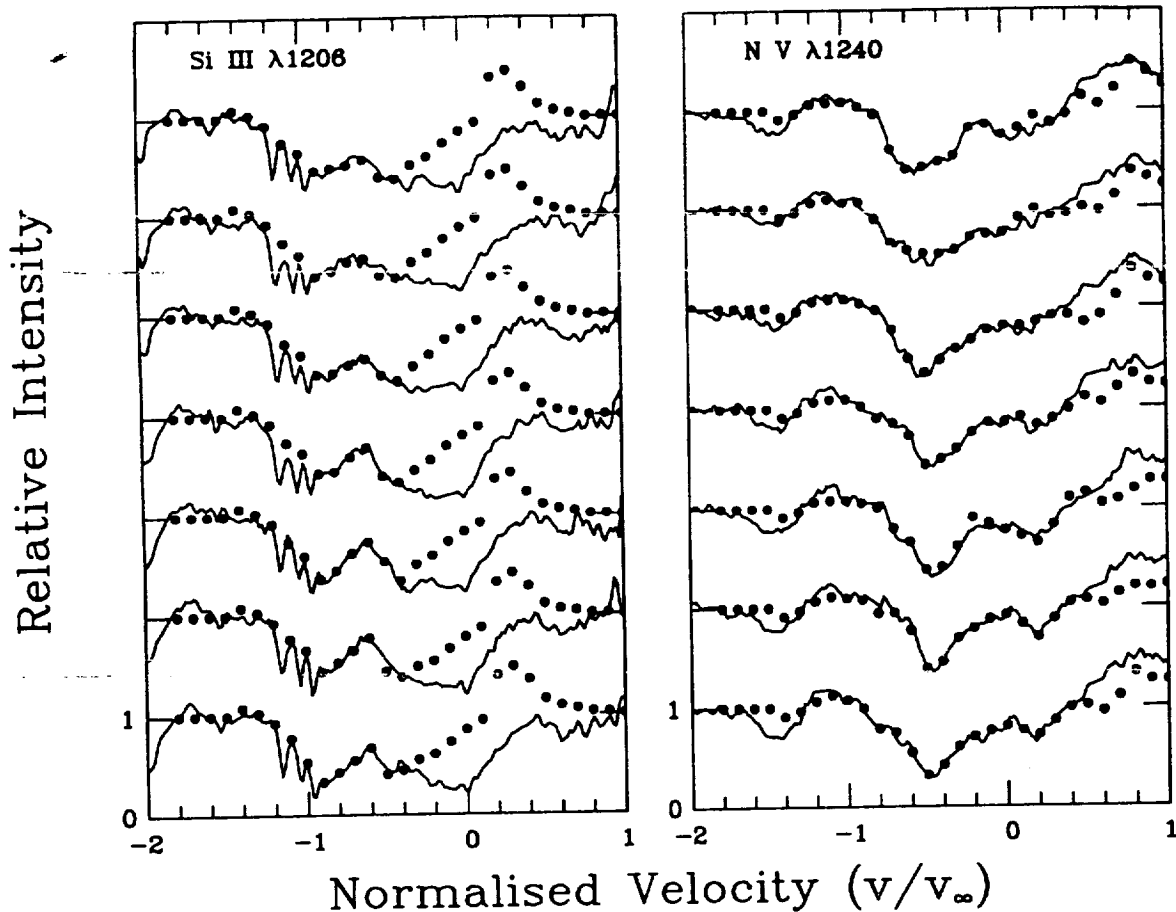
Fig. 9. Examples of profile fits (filled circles) to individual Si III λ1206 and N v λλ1240 line profiles of γ Ara (SWPs 47117 - 47257).

the wind variability on longer (multiple rotation periods) time scales.

Although not discussed in detail here, the variability of the 1995 series can be summarized as follows: considerable activity throughout the low velocity portions of the wind ($v \geq -600$ km s^{-1}); no detectable activity for $v \leq -900$ km s^{-1} (with a possible exception of one of the 17 spectra); an apparent *anti-correlation* between the activity in the lower ions such as Si III and Si IV and N v; and no evidence for modulation of the wind on the rotation time scale.

Figure 11 compares the mean spectra of several lines for the 1993 and 1995 series. While the temporal *means* of the wind lines in B supergiants such as HD 64760 do not vary with epoch (Prinja et al. 1995), several differences are clearly seen in the means shown in Figure 11. Specifically, the low ions (Al III, C II and the Si III triplets) were weaker at *all* velocities during 1995. At the same time, the high ions (Si IV, C IV and N v) weakened dramatically at high velocities but *increased* dramatically at low velocity! Thus, the observable wind was more highly ionized and more confined to lower velocities during 1995. It also appears that the emission in N v decreased slightly while the C IV emission remained constant.
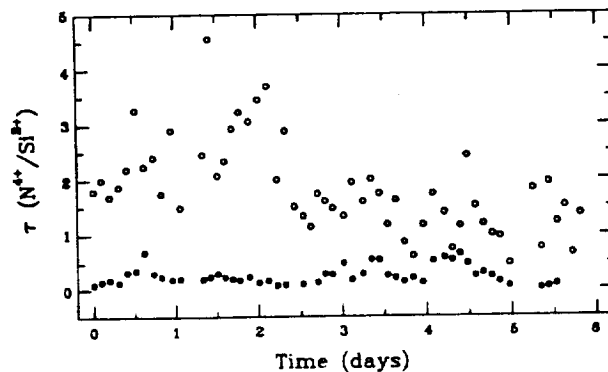

Fig. 10. The optical depth ratio of N^{4+}/Si^{2+} during the *IUE* time series is plotted, sampling high- and low-speed material at 0.7 v_{∞} (open circles) and 0.4 v_{∞} (closed circles), respectively.

Finally, we note that the profiles of the individual 1978-1982 spectra resemble the mean of the 1995 series far more than the 1993 mean. This does not seem to be a sampling effect, since fully half of the C IV profiles from the 1993 series show
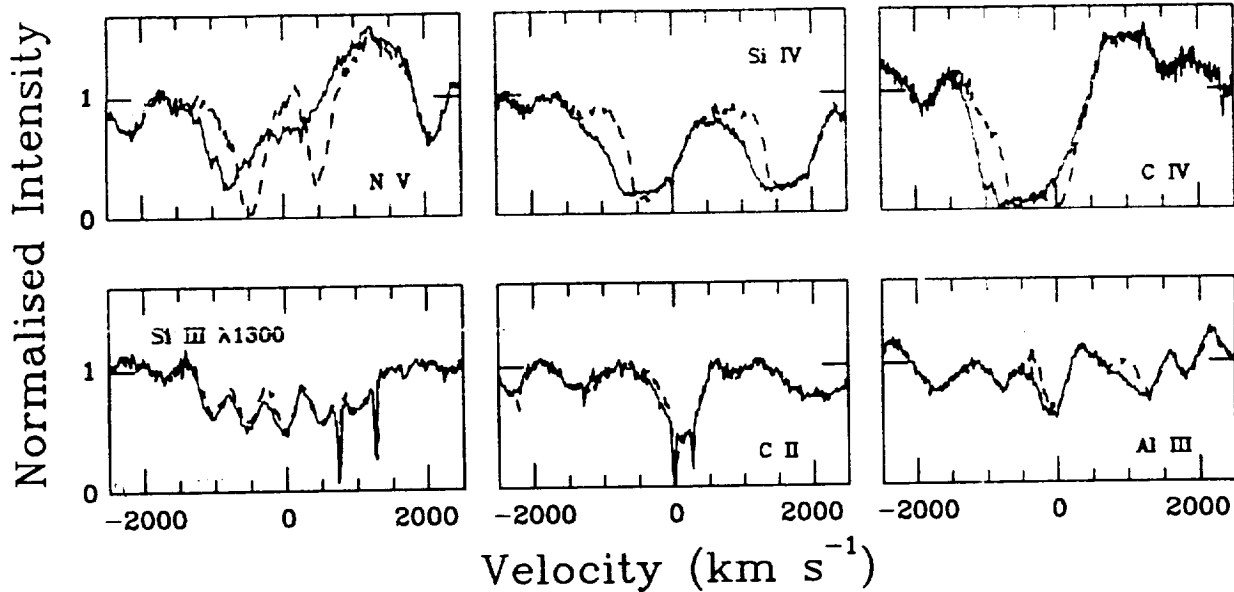
Fig. 11. A comparison between mean line profiles of γ Ara from the 1993 (solid lines) and 1995 (dashed lines) IUE time series. There is an absence of high-velocity material in the 1995 data (Section 4.4).

distinctive wind absorption shortward of -1000 km s^{-1}. Consequently, it seems that *the presence of high speed absorption is uncommon* in γ Ara.

5. A two-component stellar wind

We collate here model predictions of latitude-dependent mass-loss in rapidly-rotating hot stars, and our observational results indicating an equatorially compressed, two-component stellar wind in γ Ara. In their study of the B-type hypergiant, P Cygni, Pauldrach & Puls (1990) described a bi-stability jump for radiation-driven winds, whereby outflows which are optically thin in the Lyman continuum have a higher degree of ionization and greater terminal velocity, and winds which are optically thick in the Lyman continuum have a lower degree of ionization and a lower terminal velocity. Lamers & Pauldrach (1991) subsequently showed that this bi-stability may result in an equatorial decretion disk around rapidly-rotating, early B-type stars (i.e. at $T_{eff} \sim 21\ 000$ K), where the photospheric temperature and effective gravity is greater near the pole than the equator. The mechanism predicts an abrupt and large-scale change in overall wind structure, resulting in latitude-dependent mass-loss. Highly ionized, high-velocity material is confined to the polar regions, and gas recombines in a dense equatorial zone, leading to a less ionized, slower wind. Lamers et al. (1995) have also discussed the role of this mechanism in the formation of disks around B[e] stars.

Several results from our time-series UV analysis of wind changes in γ Ara may be compared to the model predictions of a radiatively driven two-component stellar wind:

1. γ Ara clearly has two 'terminal velocities': first, the asymptotic velocity approached by the 'Super DAC' in Si IV, Si III, N V & C IV, of ~ -750 km s^{-1}, and second, the maximum observed velocity of the migrating high speed structures (in Si IV, C IV and N V) of ~ -1500 km s^{-1}. These two velocities are close to the correct ratio predicted for the two-component stellar wind (e.g. Lamers et al. 1995).

2. The high-speed structure exists independently of the low-velocity DACs, and with different acceleration rates.

3. The lower-ionization species like Al III, C II and Si III are favoured in the low-speed wind structures.

4. The 'Super DAC' itself is highly unusual since it maintains a small line-of-sight velocity dispersion during its time evolution in any individual line, it is long-lived, has a very slow acceleration, and exhibits a clear velocity and ionization jump. Unfortunately our data set cannot be used to examine whether this feature is linked to the stellar rotation rate, since the IUE time series is not extended enough in time (Table 1). It is interesting to speculate, however, that the 'Super DAC' may relate in some manner to the interface between high- and slow-speed components which form a substantial spatially confined structure in the wind. The observed ion-dependent velocity jump may then be interpreted in terms of differences in the density, speed and ionization of material on either side of the structure (section 4.1).

5. Finally, of course, γ Ara, with its exceptional rotation rate and early B spectral type, has fundamental parameters which are consistent with the model requirements for the bi-stability mechanism.

It is interesting however to compare these time-dependent UV properties of γ Ara with those of HD 64760 (B0.5 Ib; Prinja
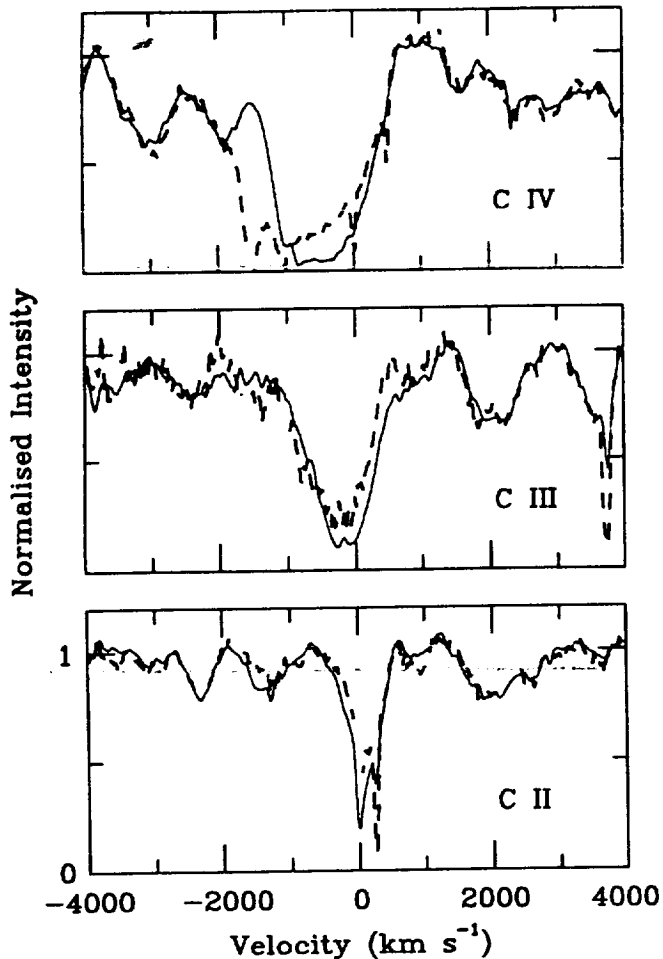
the ion mixture - relating to the onset of the bi-stability jump - is not then an obvious tracer for the differing time-variable behaviour of γ Ara and HD 64760.

We conclude therefore that the absence of significant wind ionizations changes is γ Ara compared to other B0 supergiants, plus the fact that its UV photospheric lines are essentially normal and do not indicate substantial gravity darkening, suggests that the radiative bi-stability mechanism is not the dominant contributor to the observed wind structure in γ Ara. Instead, the equatorial density enhancements are likely principally due to wind-compression effects. γ Ara is therefore a further example where a hot star wind has been distorted by the effect of rapid rotation. The result is the incidence of complex and variable wind structure. The principal characteristics of the variability are consistent with an equatorially- compressed wind, with perturbations present in the plane and at higher latitudes, independently of one another.

6. Appendix

The problem of comparing the $IU E$ observed spectra is complicated by the fact that none of them has a true continuum anywhere in the SWP wavelength range. Therefore, one must be extremely careful in normalising the spectra. We chose an approach which uses only those functional forms which are expected to affect the differences in the continuum levels of the individual spectra. These are derived and applied in order to make all of the spectra agree with one another as well as possible. Only then is a single normalising continuum adopted and applied to all of them. To obtain the relative normalisations, we account for differences in the reddening, epoch of observation (because of the time degradation of the IUE response function), and interstellar Ly α absorption. This appendix describes the details of how these adjustments were derived.

Fig. 12. The mean rectified C IV λ1550, C III λ1176 and C II λ1135 profiles of γ Ara (solid lines) and HD 64760 (B0.5 Ib; dashed lines) are compared. Despite the obviously stronger C IV profile in HD 64760, the other lines are essentially comparable.

6.1. Differential reddening corrections

We follow the prescription given by Fitzpatrick & Massa (1990; FM) to derive the extinction curves. Once the spectra have been "spun up" so that their photospheric line shapes agree with those in γ Ara, they were binned into 5 Å bins. This increases the signal-to-noise ratio, thereby avoiding the complications of lognormal statistics in the following analysis. The wavelength regions $\lambda < 1265$, $1380 < \lambda < 1415$, $1535 < \lambda < 1570$, and $\lambda > 1835$ were excluded from the analysis to eliminate the effects of wind lines, Ly α, and the poorly determined region shortward of Ly α. The fluxes, $f(\lambda)$, were then converted into magnitudes by the relation $m(\lambda) = -2.5 \log_{10} f(\lambda) - 21.1$ and the V magnitude was subtracted to form colors, $m(\lambda - V) \equiv m(\lambda) - V$. The colors were then used to create differential extinction curves,

et al. 1995, Massa et al. 1995b), which is also a rapid rotator with a highly active and structured wind. In the case of HD 64760, however, there is no clear indication of a rotationally distorted outflow, though structures are seen which co-exist on separate time scales. Lamers et al. (1995) concluded that in their sample of hot stars the 'bi-stability jump' found near $T_{\rm eff} \sim 21\ 000K$ is related to a significant change in wind ionization near spectral types B1. Following Lamers et al. (see their Fig. 8), we compare in Fig. 12 the mean rectified C IV λ1550, C III λ1176 and C II λ1135 profiles of γ Ara and HD 64760 (from the 'MEGA' collection of Prinja et al. 1995). Despite the fact that HD 64760 has a higher wind terminal velocity and a stronger C IV profile, the lower-ion species are basically comparable; i.e., γ Ara does not exhibit a substantially stronger C II profile for example. It seems, therefore, that in this case the degree of wind ionization is not correlated to the terminal velocity. A marked change in

$$k(\lambda - V) = \frac{m(\lambda - V)_c - m(\lambda - V)_\gamma}{(B - V)_c - (B - V)_\gamma}. \tag{2}$$

where the subscript γ refers to the γ Ara colors and c refers to the comparison star. The resulting curves were fitted by the FM functional

form (eqs [2]-[4] in FM) except that the central position of the 2175 Å bump was fixed at 2174 Å (4.6 μm^{-1}) since it rarely shifts and is poorly determined by fluxes in the SWP region.

The ζ Per fluxes were multiplied by a factor of 1.5 to account for the fact that it is a small aperture spectrum. As long as this factor is within a 10-20% of the actual amount, it should not affect the fitting procedure, although it may affect the values of the derived parameters.

Because only the short wavelength wing of the 2175 Å bump is present in the SWP range, the derived bump quantities are expected to be unreliable. The coefficients used in the differential extinction corrections are listed in Table 2.

6.2. Time degradation corrections

Although temporal degradation of the *IUE* response is well documented for the low dispersion modes (Garhart 1992 – *IUE* Newsletter No. 48), its effects have not been quantified for the high resolution modes. Consequently, we had to determine our own degradation function. We estimated the degradation by comparing the SWP 7718 spectrum of HD 64760 (obtained 20 Jan 1980) to the mean of the 148 spectra for this star obtained in 13-29 Jan 1995 as part of the *IUE* MEGA project (Prinja et al. 1995). The magnitude and wavelength dependence of time degradation over this 15 yr baseline are similar to the low resolution functions derived by Garhart (1992, see also Howarth & Smith 1994). The strongest effects of degradation are shortward of Ly α. This enabled us to first obtain a reddening correction, and then determine the degradation correction by dividing the reddening corrected spectra by a power (< 1) of the function of the degradation. Once a power was determined which brought the short wavelength fluxes of the comparison stars into agreement with γ Ara, we then applied the degradation correction and redetermined the reddening correction. This procedure was iterated to convergence (2-3 iterations). Nevertheless, because the degradation correction is large shortward of Ly α, the flux levels there should be regarded with caution. The final values for the power needed to obtain agreement are 0.6 for SWP 38782 (obtained 13 May 1990) of HD 109867 and 0.8 for SWP6454 (obtained 9 Sept. 1979) of ζ Per. The values of the powers are consistent with the rank ordering of the intervals between the observations (1 for 15 years, 0.8 for 13.5 yrs, and 0.6 for 2.8 yrs), but the power for the HD 109867 seems a bit large.

6.3. Ly α corrections

The final step in adjusting the comparison spectra was to correct for the influences of differential Ly α absorption. In this case, we simply divided the corrected comparison spectra by different multiples of the Ly α profile function (see FM) until we determined a value that caused the wings of the interstellar Ly α to agree. The resulting column densities are given in Table 2, and are comfortably within the errors of the values listed by Diplas and Savage (1994). Note that even though ζ Per is more reddened than HD 109867, it required less differential correction. This is because much of the hydrogen along its line of sight is in molecular form (Bohlin, Savage & Drake 1978).

Table 2. Relative extinction parameters

Star	$\Delta N(H\ I)\ cm^2$	γ	a_1	a_2	a_3	a_4
ζ Per	0.2×10^{20}	1.311	-0.1828	0.816	4.921	0.7168
HD 109867	7.0×10^{20}	1.085	0.4136	0.782	5.630	0.5407

References

Baade D. 1983, A&A, 124, 211

Baade D., Ferlet R. 1984, A&A, 140, 72

Bjorkman J.E., Cassinelli J.P. 1992, in Nonisotropic and Variable Outflows from Stars, ed. Drissen, L., Leitherer, C., Nota, A. (A.S.P. San Francisco), A.S.P. Conf. Series 22, 88

Bjorkman J.E., Cassinelli J.P. 1993, ApJ, 409, 429

Bjorkman J.E., Ignace R., Tripp T.M., Cassinelli J.P. 1994, ApJ, 435, 416

Bohlin R.C., Savage B.D., Drake J.F. 1978, ApJ, 224, 132

Cassinelli J.P., Waldron W.L., Sanders W.T., Harden F.R., Rosner J.R., Vaiana G.S. 1981, ApJ, 250, 677

Cranmer S.R., Owocki S.P. 1996, ApJ, in press

Diplas A., Savage B.D. 1994, ApJS, 93, 211

Fitzpatrick E.L., Massa D. 1990, ApJS, 72, 163 (FM)

Garhart 1992, NASA IUE Newsletter No. 48, p.98

Giddings J.R., Rees P.C.T., Mills D., Clayton M.J. 1995, Starlink User Note 37 (Didcot: PPARC, Rutherford Appleton Lab.)

Grillo F., Sciortino S., Micela G., Vaiana G.S., Harnden F.R. 1992, ApJS, 81, 795

Hiltner W.A., Garrison R.F. Schild R.E. 1969, ApJ, 157, 313

Howarth I.D., Bolton C.T., Crowe R.A., Ebbets D.C., Fieldus M.S., Fullerton A.W., Gies D.R., McDavid D., Prinja R.K., Reid A.H.N., Shore S.N., Smith K.C. 1993, ApJ, 417, 338

Howarth I.D., Prinja R.K. 1989, ApJS, 69, 527

Howarth I.D., Reid A.H.N. 1993, A&A, 279, 148

Howarth I.D., Smith K.C. 1994, ApJ, 439, 431

Howarth I.D., Prinja R.K., Massa D. 1995, ApJ, 452, L65

Humphreys R.M., McElroy D.B. 1984, ApJ, 284, 565

Lamers H.J.G.L.M., Cerruti-Sola M., Perinotto, M. 1987, ApJ, 314, 726

Lamers H.J.G.L.M., Pauldrach, A.W.A. 1991, A&A, 244, L5

Lamers H.J.G.L.M., Snow T.P., Lindholm, D.M. 1995, ApJ, 455, 269

Lucy L.B. 1982, ApJ, 255, 278

Lucy L.B. 1983, ApJ, 274, 372

Massa D. 1992, in Nonisotropic and Variable Outflows from Stars, ed. Drissen, L., Leitherer, C., Nota, A. (A.S.P. San Francisco), A.S.P. Conf. Series 22, 84

Massa D. 1995, ApJ, 438, 376

Massa D. et al. 1995a, ApJ, 452, L53

Massa D., Prinja R.K., Fullerton A.W. 1995b, ApJ, 452, 842

Massa D., Shore S.N., Wynne, D. 1992, A&A, 264, 169

Mullan D.J. 1984, ApJ, 283, 303

Owocki S.P., Castor J.I., Rybicki G.B. 1988, ApJ, 335, 914

Owocki S.P., Cranmer S.R., Blondin J.M. 1993, ApJ, 424, 887

Pauldrach A.W.A., Puls J. 1990, A&A, 237, 409

Petrenz P., Puls J. 1996, A&A, in press

Prinja R.K. 1994, in Pulsation, Rotation and Mass Loss in Early-Type Stars, ed. Balona, L.A., Henrichs, H.F. Le Contel, J.M. (Kluwer: Dordrecht), IAU Symp. 162, 507

Prinja R.K., Howarth I.D. 1986, ApJS, 61, 357

Prinja R.K., Barlow M.J., Howarth, I.D. 1990, ApJ, 3661, 607

Prinja R.K., Massa D., Fullerton A.W. 1995, ApJ 452, L61

Puls J., Owocki S.P., Fullerton A.W. 1993, A&A, 279, 457

Reid A.H.N., Howarth I.D. 1996, A&A, in press

Slettebak, A. Collins G.W. II., Boyce P.B., White N.M., Perkinson T.D. 1975, ApJS, 29, 137

Snow T.P. 1977, ApJ, 217, 760

Snow T.P., Morton D.C. 1976, ApJS, 32, 429

Uesugi A., Fukuda, L. 1982, *Revised Catalogue of Stellar Rotational Velocities* (Kyoto: Department of Astronomy, Kyoto University)

Walborn N.R. 1976, ApJ, 205, 419

Walborn N.R., Panek R.J. 1985, ApJ, 291, 806

Walborn N.R., Parker J.W., Nichols J.S. 1995, *International Ultraviolet Explorer Atlas of B-Type Spectra from 1200 to 1900 Å*, (NASA Ref. Pub. 1363)

Enclosure 6

18.06

The Peculiar Atmospheric Composition of the DO White Dwarf MCT 0501-2858

E. F. Polomski (U Fl), S. Vennes. P. Chayer (CEA, UCB)

MCT 0501-2858 is a helium rich DO white dwarf (T=70,000K, log g =7.0) discovered in the Montreal-Cambridge-Tololo (MCT) survey of blue southern hemisphere objects (Vennes *et al.* 1994, ApJL, 421, L35). DO white dwarfs are much rarer than hydrogen rich DA types and may represent an earlier stage in the evolution of these objects. Additional study of this object with the *Voyager* probe and *EUVE* satellite revealed that it is located at an unusually low ISM column density (Barstow *et al.* 1994, MNRAS, 267, 653; Vennes *et al.* 1994).

We report identification of the strongest spectral lines in the high-resolution *IUE* (1150-1950 Å) spectrum of this object and the results of LTE model atmosphere fitting to the elemental abundances. The ultraviolet spectrum of this object is characterized by weak, low ionization ISM lines and strong photospheric lines of C III λ 1247, C IV $\lambda\lambda$ 1230, 1548, 1550, N IV λ 1718, N V $\lambda\lambda$ 1239, 1243, O IV $\lambda\lambda$ 1338, 1343, O V λ 1371, and Si IV $\lambda\lambda$ 1393, 1402.

We derive abundances with respect to helium by number of 3×10^{-3}, 6×10^{-5}, 3×10^{-3}, and 6×10^{-5}, for C, N, O, and Si, respectiveley. We find an excess of C and O (C/He=0.5 solar O/He = .3 solar) relative to all other elements. N and Si are present at .03 solar and .12 solar respectiveley. MCT 0501-2858 is lacking in Fe and an upper limit has been obtained for the abundances of both Fe and Ni of 1×10^{-6}. Given the high C and O abundances, one would expect similar amounts of Fe and Ni, but they are not apparent in the spectra, contrary to what is observed in DA white dwarfs of similar temperature (Holberg *et al.* 1994, ApJL, 425, L105). We present a detailed comparison of the abundances derived from synthetic FUV and EUV models to the *IUE* and *EUVE* data (Vennes *et al.* 1994, BAAS, 26, 868). Higher resolution spectra are hoped for with *HST* to refine the Ni and Fe abundances. This work has been supported by NASA grant NAG5-2405.

Session 19: Hot Stars
Display Session, 10:00am-6:30pm
Convention Center, North Banquet Hall

19.01

Accurate Classification of Two-Dimensional Spectra with Artificial Neural Networks

W.B.Weaver and A.Torres-Dodgen (MIRA)

We have designed a suite of Artificial Neural Networks (ANNs) that are able to classify accurately the near-infrared spectra of ordinary stars in temperature and luminosity. The temperature classes O - M and luminosity classes Ia - V are classified in the extension of the MK System in the silicon-accessible (peak CCD and Reticon sensitivities) near-infrared ($\lambda\lambda$5800—-8900). This classification system (Torres-Dodgen and Weaver, 1993, PASP, 105, 693) is rigorously based on MK standards.

Although we employ only 15 Å resolution spectra, the ANNs achieve fractional sub-class temperature and luminosity accuracies comparable to those obtained by expert classifiers with 2 Å resolution photographic spectra. Even OB stars are well classified by this system. We have demonstrated previously (Weaver and Torres-Dodgen, 1995, ApJ. 446, 300 and references therein) that ANN classification can detect, and classify the components of, binary stars; can accurately determine interstellar reddening during classification; and degrades slowly with decreasing signal-to-noise ratios. The remaining issue is to determine the limit of spectral peculiarities that can be detected by ANNs at these resolutions.

Such ANNs can be used for automated spectroscopic surveys that are as accurate but two magnitudes deeper than spectroscopic surveys using expert human classifiers.

19.02

Analysis of the Line Variations in the Wind of HD 160529

Th.Gäng, C.Leitherer (STScI), B.Wolf, O.Stahl, A.Kaufer, Th.Rivinius, C.Gummersbach, H.Mandel, J.Feitz, Th.Szeifert (LSW), J.Kovacs, I.Jankovics (GAO)

We have observed the galactic Luminous Blue Variable (LBV) HD 160529 with a spectral resolving power of $R \sim$ 20 000 in the wavelength range 3450 Å $< \lambda < $ 8650 Å. The observations were carried out with a fiber-linked echelle spectrograph at the ESO 50-cm telescope in La Silla from 1992 to 1995. In total over 200 spectra were obtained; each spectra with S/N $\sim$ 100 around 5500 Å.

We found that all spectral lines are variable. The lines with P Cygni-type profiles show variations in the emission as well as in the absorption components. Even pure absorption lines, forming deep in the atmosphere (e.g. He I λ5876 and Mg II λ4481), show signs of wind-influence, indicating that the observed variations are caused at the very base of the wind (e.g. by propagating density fluctuations starting at the photosphere).

The data is analyzed with the latest NLTE-codes of Hubeny *et al.* (TLUSTY, SYNSPEC) to get reliable stellar parameters. The NLTE-results are compared with the output from other numerical codes in order to examine the significance and effects of the various parameters (LTE, spherical symmetry, wind,...) on the calculated synthetic atmospheres.

Finally we use the results from the previous (static) models as input for recently developed dynamical models (SEIDYNAMIC/Rivinius *et al.* 1995) to reconstruct the time-dependence of the observed line-profile variations.

19.03

Stellar Wind Variability: The Things B Supergiants Do

Derck Massa (ARC), Alex Fullerton (MPIA, München), Raman Prinja (UCL)

We discuss why B supergiant winds are particularly well suited for wind variability studies, and then present a gallery of dynamic spectra which demonstrate the range of wind variability observed in B supergiants. The examples suggest the presence wind compressed disks, bifurcated winds, shock formation, rotationally modulated winds and the spontaneous generation of wind enhancements. They underscore the strength and richness of wind variability in B supergiants and the challenges these phenomena present to theoretical studies of stellar winds.

19.04

The Erratic Behavior of C II 4267 in Early B Stars

R.F. Garrison and D. Hamilton (David Dunlap Obs., U. Toronto)

Classification spectra (1-3 Å resolution) of early B stars give an impression that the CII 4267 line is unreliable as a classification criterion. Its erratic behaviour is quite unlike OII or NII lines which are relatively well behaved and vary predictably with temperature and log g. In fact, even other lines of CII such as 6578 and 6582 are much more predictable than 4267. Models (e.g. Lennon, *et al.*, 1983; Eber and Butler, 1988) indicate that non-LTE effects may be the cause of the erratic behavior. We have confirmed and quantified this impression using a large database of 788 photographic spectra of 512 well-classified stars, as well as multiple high-resolution CCD spectra of 13 stars. No variability greater than 5spectra over timescales of hours, days, weeks, or months, and no major changes were observed in the photographic spectra over years. While there is some vague correlation with temperature and log g, it is not possible to account for the large scatter observed without invoking something like non-LTE.

MONDAY